



RESEARCH LETTER

10.1029/2018GL080135

Key Points:

- Average wintertime near-surface wind convergence over Kuroshio Extension and Gulf Stream is a direct accumulation of a baroclinic waveguide
- Baroclinic waveguide contribution to time-mean convergence decomposed into atmospheric frontal and non-frontal scenarios
- Distinction suggests a new paradigm for understanding mechanisms of ocean-atmosphere forcing in western boundary current regions

Supporting Information:

- Supporting Information S1

Correspondence to:

R. Parfitt,
rparfitt@whoi.edu

Citation:

Parfitt, R., & Seo, H. (2018). A new framework for near-surface wind convergence over the Kuroshio Extension and Gulf Stream in wintertime: The role of atmospheric fronts. *Geophysical Research Letters*, 45. <https://doi.org/10.1029/2018GL080135>

Received 20 AUG 2018

Accepted 13 SEP 2018

Accepted article online 17 SEP 2018

A New Framework for Near-Surface Wind Convergence Over the Kuroshio Extension and Gulf Stream in Wintertime: The Role of Atmospheric Fronts

Rhys Parfitt¹  and Hyodae Seo¹ 

¹Woods Hole Oceanographic Institution, Woods Hole, MA, USA

Abstract It is well known that the wintertime time-mean surface wind convergence patterns over the Kuroshio Extension and Gulf Stream show significant imprints of the underlying oceanic fronts. Previous studies have suggested that this collocation results from a time-mean response to sea level pressure forcing from sea surface temperature gradients. However, more recent work has illustrated this phenomenon is heavily influenced by extratropical cyclones, although exact mechanisms are still debated. The purpose of this study is to introduce a new framework that explicitly distinguishes between two separate components in their contribution to the time-mean surface wind convergence, that associated with and without atmospheric fronts. It is then argued that this distinction can help better explain the mechanisms driving the Kuroshio Extension and Gulf Stream influence on the atmosphere.

Plain Language Summary This paper presents a new framework for understanding the mean wintertime atmospheric state over the Kuroshio Extension and Gulf Stream regions, in the context of advancing our understanding of how these strong ocean currents can impact on the seasonal atmosphere. In recent years, many studies have attributed the oceanic imprint on the atmosphere in these regions to mechanisms based upon the time-mean response. However, observational analysis here illustrates that the regional wintertime atmosphere is, in fact, dominated by continuous extratropical storm systems. It is suggested this contribution to the mean atmospheric state can be further decomposed into situations when atmospheric fronts embedded within these storms are and are not present. By studying each of these distinct atmospheric scenarios, it is then argued that the oceanic imprint on the mean wintertime atmospheric state should instead be considered as an accumulation of processes driven by mechanisms acting on a synoptic timescale, not on the timescale of the time-mean. This framework presents a new paradigm for understanding extratropical frontal-scale air-sea interactions and is expected to have an immediate impact on atmospheric, oceanic, and climate communities.

1. Introduction

Over the past few decades, there has been a steadily growing body of evidence suggesting that ocean mesoscale and frontal-scale features in the Kuroshio Extension (KE) and Gulf Stream (GS) regions are forcing the atmosphere (e.g., Chelton et al., 2004; Kuwano-Yoshida & Minobe, 2017; Ma et al., 2016; Piazza et al., 2016; Seo et al., 2017; Small et al., 2014; Xie, 2004). In particular, a positive correlation between sea surface temperature (SST) and near-surface wind speed over western boundary currents (WBCs) suggest an ocean-to-atmosphere forcing through turbulent heat fluxes (Nonaka & Xie, 2003), whose variability on monthly and longer timescales is largely driven by internal ocean processes (Bishop et al., 2017). Studies considering the atmospheric impact of WBCs typically fall into one of two broad categories—the oceanic impact on the mean state (e.g., Shimada & Minobe, 2011) and on synoptic storms (e.g., Hirata et al., 2015, 2018), with community efforts still very much ongoing (e.g., Nkwinkwa Njouodo et al., 2018; Small et al., 2018). One major outstanding issue, however, is a lack of mechanistic understanding concerning how these two distinct research avenues coalesce.

A clear example is the pronounced band of near-surface wind convergence (NSWC) in the time-mean, which is observed to meander along the strong SST gradients of the KE and GS (e.g., Feliks et al., 2004, 2007; Kobashi et al., 2008; Minobe et al., 2008, 2010; Tokinaga et al., 2009). This meandering also imprints on the time-mean local precipitation rate, as well as on the tropospheric vertical velocity field. Many potential contributors have been put forward to explain this time-mean atmospheric response (see Small et al., 2008, for a broad

overview). Perhaps the two mechanisms traditionally discussed the most in the literature are the *momentum mixing* anomalies induced down through the boundary layer by differential SST values (Hayes et al., 1989; Wallace et al., 1989) and the *pressure adjustment mechanism* (Lindzen & Nigam, 1987; Minobe et al., 2008) whereby flux-driven spatial pressure gradients drive secondary circulations (Wai & Stage, 1989). Kilpatrick et al. (2014) and Schneider and Qiu (2015) argue that these mechanisms depend on the background wind speed, while Liu et al. (2013) suggest that these mechanisms are timescale dependent, with the pressure adjustment mechanism dominating in time-mean due to synoptic vector wind perturbations averaging out.

However, in wintertime, it is known that a *baroclinic waveguide* exists in the midlatitudes (Chang et al., 2002; Wallace et al., 1988), within which a continuous series of low- and high-pressure systems propagate. Recently, new studies (O'Neill et al., 2017; Parfitt & Czaja, 2016) have emerged suggesting that this band of time-mean NSW and associated upward vertical motion is, in fact, a direct accumulation of synoptic vector winds, not the consequence of cancellation in synoptic vector wind perturbations. O'Neill et al. (2017) note that these results are difficult to reconcile with the notion that SST anchors NSW through a local boundary layer adjustment mechanism. Plougonven et al. (2018) argue that while these results do indicate the importance of synoptic transients, they may nevertheless not completely rule out the existence of a semi-permanent SST front signal in the NSW field. Indeed, Vanni re et al. (2017) proposed a *cold-path* mechanism that illustrates the influence of the GS SST front on the cold sector of extratropical storms based on a modified version of the pressure adjustment mechanism from Minobe et al. (2008). O'Neill et al. (2018) conclude that the community is still searching for a robust diagnostic, uncontaminated by storm-track variability, that demonstrates the coupled air-sea response in WBCs, or as they earlier describe, "a robust diagnostic that removes storm-track variability [...] while retaining the comparatively weak SST-induced signal."

It is the specific aim of this paper to illustrate that the atmospheric fronts embedded within passing synoptic storms are a suitable candidate for this robust diagnostic over the KE and GS in wintertime. In the context of the NSW, this allows one to adopt a framework separating the time-mean NSW into two fundamental meteorological constructs related to the waveguide, as introduced in Parfitt and Czaja (2016). The first of these is potential vorticity-induced isentropic upglide and downglide (see Figure 1 of Hoskins et al., 2003), which is expected to offer a significant degree of cancellation. The second of these is the diabatic contribution expected to take place in the small part of the system where condensation is present (Emanuel, 1985), outside of which the descent is cloud-free and slow, determined by radiative heat loss (Green et al., 1966). A large portion of this second contribution takes place at the atmospheric front embedded within the extratropical cyclone, essentially suggesting the decomposition of the NSW field into atmospheric frontal and non-frontal scenarios. It is noted that this distinction between atmospheric frontal and non-frontal situations also makes sense in the context of previous observational and modeling studies showing the KE and GS impact on rainfall (e.g., Hand et al., 2014; Sasaki et al., 2012), as atmospheric fronts are known to account for up to 90% of the rainfall variability in these regions (Catto et al., 2012).

The data and method used in this study are described in section 2. Reanalysis composites of NSW in atmospheric frontal and non-frontal situations are shown and discussed in section 3. A summary and discussion of the implications for SST forcing of the KE and GS on the atmosphere are provided in section 4.

2. Data and Method

The data set used in this study is the National Centers for Environmental Prediction Climate Forecast System Reanalysis (NCEP-CFSR) product (Saha et al., 2010). NCEP-CFSR has a global atmospheric spectral resolution T382 (~38 km) and is provided on a $0.5^\circ \times 0.5^\circ$ longitude-latitude grid. NCEP-CFSR is based on a coupled data assimilation incorporating a global ocean model with the horizontal resolution of 0.25° , extending to 0.5° toward the poles. The period of analysis considered in this study is December–February (DJF), 1979–2010. *Near-surface* wind convergence will be taken at the 900 hPa level.

For the calculation of atmospheric fronts, the F diagnostic, $F = \frac{\zeta_p |\nabla(T_p)|}{\zeta_o |\nabla T_o|}$, where $|\nabla(T_p)|$ is the magnitude of the temperature gradient on pressure level p , ζ_p is the isobaric relative vorticity on that same pressure surface, ζ_o is the Coriolis parameter at each latitude, and $|\nabla T_o|$ is a typical scale for temperature gradient $0.45 \text{ K}/100 \text{ km}$, is used (Parfitt, Czaja, & Seo, 2017). For the pressure level considered in this study, 900 hPa, frontal regions are identified where the variable F exceeds a value of 1. This choice of threshold has been verified in Parfitt, Czaja,

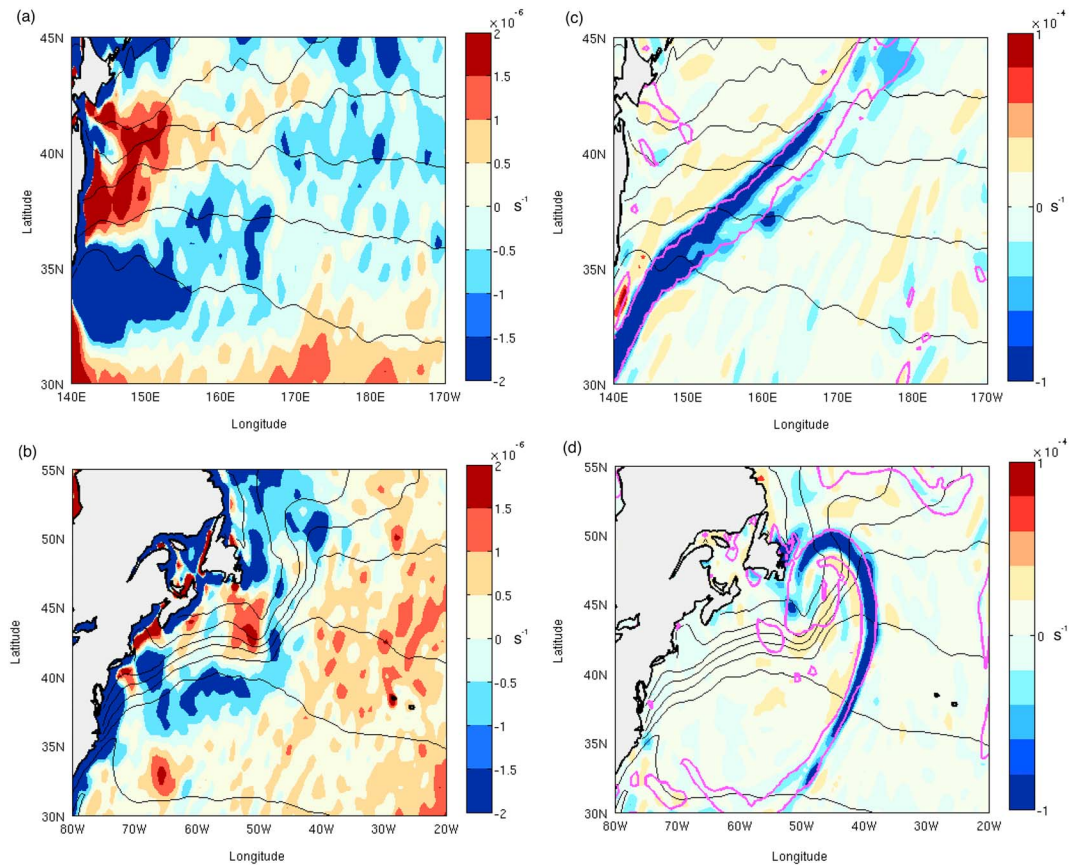


Figure 1. The time-mean near-surface wind convergence/divergence field for the period December–February 1979–2010 over the Kuroshio Extension and (b) Gulf Stream. The coastline is plotted as a thick black line and the continent masked in gray. The time-mean sea surface temperature contours for the same period are also plotted as thin black lines from 3 to 24 °C at 3 °C intervals. Instantaneous snapshots of the near-surface wind convergence/divergence field are shown at (c) 0000 UTC on 24 December 1979 over the Kuroshio Extension and (d) 0000 UTC on 12 February 1980 over the Gulf Stream. Atmospheric fronts, identified where the variable F exceeds a threshold of 1, are highlighted in magenta.

and Seo (2017) through extensive manual analyses and comparison with the objective metric from Hewson (1998). The F diagnostic has been recently employed in a wide variety of other studies (e.g., Messori et al., 2017; Parfitt, Czaja, & Kwon, 2017; Sasaki & Yamada, 2017), and temperature gradient and relative vorticity variables have also been used for more general frontal activity metrics (Solman & Orlanski, 2010). It is noted that the main conclusions of this study do not change if one employs the diagnostic from Hewson (1998) instead.

3. Results

3.1. Time-Mean and Snapshot NSWC/NSWD

Figure 1 illustrates the time-mean NSWC/near-surface wind divergence (NSWC/NSWD) fields for the period DJF 1979–2010 over the (a) KE and (b) GS, with the time-mean SSTs superimposed to illustrate the regions of strong SST gradients. In all figures in this paper, the convention is adopted that positive (negative) shading denotes NSWD (NSWC). As has been previously observed, patterns of NSWC are located on the warm side of the strong SST gradients, on the order $2 \times 10^{-6} \text{ s}^{-1}$. The strongest time-mean NSWC is found in the KE region, accompanied on the cold side of the SST front by a NSWD of the same magnitude. In the GS region, the time-mean NSWC is slightly lower, with the corresponding NSWD mostly localized near the region $\sim 50^\circ\text{W}$, 42°N . Large time-mean values of both NSWC and NSWD are observed close to land due to the effect of coastlines on the near-surface wind fields.

Despite the noticeable imprint of both the KE and the GS SST fronts on the time-mean NSWC, however, as pointed out in Parfitt and Czaja (2016) and O'Neill et al. (2017), the time-mean atmospheric state in these regions is heavily skewed toward the contribution from extreme tail end values an order or two of magnitude larger than observed in the mean; specifically, the contribution from synoptic weather systems. Consequently, on any individual day, these patterns are rarely recovered. This can be clearly seen in Figure 1, which also illustrates snapshots of the 900 hPa NSWC/NSWD for (c) 0000 UTC on 24 December 1979 over the KE and (d) 0000UTC on 12 February 1980 over the GS. In each snapshot, the NSWC is noticeably dominated by features with values on the order of 10^{-5} s^{-1} up to maxima of 10^{-4} s^{-1} , typically concentrated in thin elongated spatial regions, with widths on the order of 100 km. On each individual figure, atmospheric fronts are also overlaid in magenta as contours encompassing regions where $F > 1$. As can be seen, there is a high degree of correspondence between the areas of strongest NSWC and atmospheric frontal regions. Outside of these atmospheric fronts, broader areas of NSWD and NSWC are observed with the order of 10^{-5} s^{-1} —still an order of magnitude higher than observed in the time-mean. To further understand this distinction, the time-mean of atmospheric frontal and non-frontal situations is considered.

3.2. Time-Mean NSWC/NSWD in Atmospheric Frontal and Non-frontal Situations

Figure 2a illustrates the composite wintertime NSWC/NSWD at each grid point whenever an atmospheric front is identified in DJF. As one might expect, there is no composite NSWD observed anywhere. The average value of NSWC is distributed somewhat evenly across each oceanic basin with values ranging from 2×10^{-5} to $3 \times 10^{-5} \text{ s}^{-1}$. However, slightly higher values are observed on the warmer side of the sharp SST fronts, especially across the GS (see supporting information Figure S1 for regional close-up). Although the influence of the KE and GS on the North Pacific and North Atlantic storm-tracks is becoming well documented (Joyce et al., 2009; Nakamura et al., 2012; Taguchi et al., 2009), little has been studied on the impact on atmospheric fronts. In a study by Parfitt et al. (2016), perturbations to the sharp SST gradient in the GS were found to invoke a strong response on surface atmospheric frontal development, mediated by the induced change in cross-frontal surface sensible heat flux. This mechanism, termed “Thermal Damping and Strengthening” (TDS), depends on the SST gradient and the relative orientation of the atmospheric and oceanic front. As such, the fact that the GS SST front is sharper (except between 140°E and 150°E where the KE contrast in atmospheric frontal NSWC is most clear) and more aligned with the land-sea boundary than the KE SST front may explain why the difference in atmospheric frontal NSWC magnitude between the warm and cold sides of the GS is more prominent than between the warm and cold sides of the KE. While the average NSWC composite magnitude for atmospheric fronts is a few times smaller than the maximum values observed in Figures 1c and 1d, this is expected as these maxima are not observed along the whole extent of an atmospheric front. A reference for the fraction of wintertime days (i.e., the atmospheric frontal frequency) to which this composite reflects can be found in Figure 2a of Parfitt, Czaja, and Seo (2017). Atmospheric frontal frequencies in DJF at 900 hPa generally reach a maximum over the KE and GS of up to $\sim 25\%$.

Figure 2b illustrates the composite wintertime NSWC/NSWD for atmospheric non-frontal situations (i.e., whenever an atmospheric front is not present), plotted on the same color scale as Figure 2a. This non-frontal composite reflects the average NSWC/NSWD over the KE and GS over $\sim 75\%$ of the time. As can be seen, the average non-frontal NSWC/NSWD is globally much lower in magnitude than the NSWC/NSWD in frontal situations, and at this scale, there are no observable structures present. Figure 2c plots the same non-frontal NSWC/NSWD, except the color scale is reduced by a factor of five. At this scale, it is clear that, except for at a handful of coastal grid points, on average there is instead NSWD located everywhere. In other words, the removal of the average atmospheric frontal signal in NSWC leaves a much weaker signal of opposite sign (in NSWD) in which the meandering imprint of the KE and GS can still be seen.

At this stage, it is insightful to further decompose the atmospheric non-frontal NSWC/NSWD into situations where we find NSWC and NSWD separately. Figure 3a illustrates the percentage of wintertime days where non-frontal NSWC is detected at each grid point. Although on average there is NSWD located everywhere on non-frontal days, across the KE and GS SST fronts NSWC is found on around $\sim 25\text{--}30\%$ of these non-frontal days. Outside of these sharp SST frontal regions this fraction increases to $\sim 40\%$ of the time. Figure 3b (3c) illustrates the composite NSWC (NSWD) at each grid point on non-frontal days where there is NSWC only (NSWD only). It can immediately be seen that while the average NSWC/NSWD across all non-frontal days is on the order of 10^{-6} s^{-1} , the respective non-frontal NSWC-only and NSWD-only composites

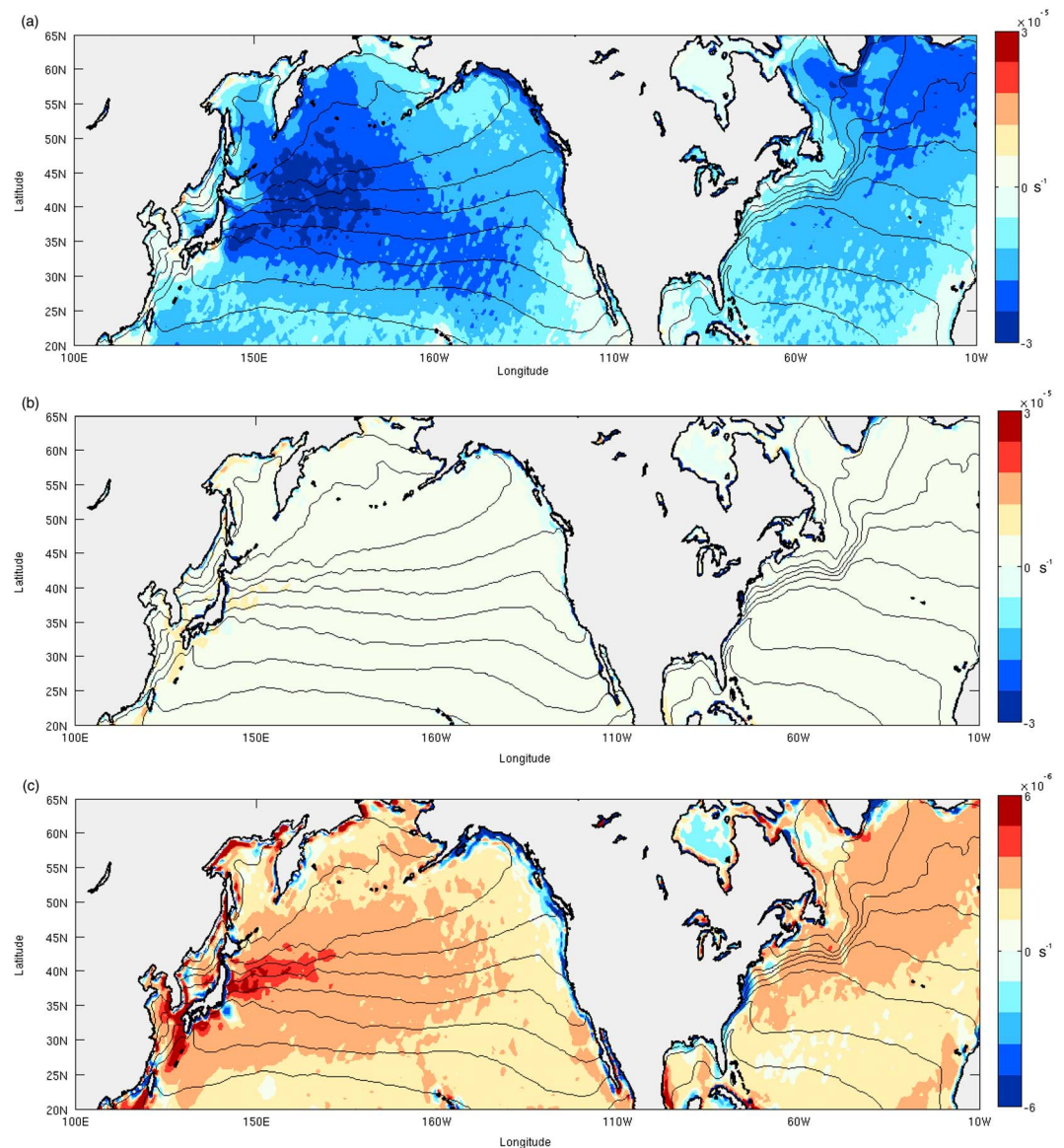


Figure 2. The time-mean near-surface wind convergence/divergence field over the Kuroshio extension and Gulf Stream for the period December–February 1979–2010 when (a) atmospheric fronts only are present (atmospheric frontal) and (b) when atmospheric fronts are absent (atmospheric non-frontal). (c) As in (b) except the color scale is reduced by a factor of 5. The time-mean sea surface temperature contours for the same period are also plotted as thin black lines from 3 to 24 °C at 3 °C intervals.

are on the order of 10^{-5} s^{-1} . In other words, the average non-frontal NSWC/NSWD is the residual of non-frontal NSWCs and NSWDs an order of magnitude larger, as is found within synoptic storms. It is suggested here that this decomposition confirms the hypothesis put forward by Parfitt and Czaja (2016) that the time-mean NSWC/NSWD field is set by the continuous baroclinic waveguide known to exist in these regions and that the baroclinic waveguide can be decomposed using well-established meteorological constructs into the following:

1. The contribution from isentropic upglide/downglide within which a large degree of cancellation is expected (Figures 2c, 3b, and 3c). This is illustrated schematically in supporting Figure S2a, which shows the vertical motion associated with isentropic upglide and downglide induced by a sharp positive potential vorticity anomaly superimposed on a westerly flow (cf. Figure 1; Hoskins et al., 2003). Sharp mid-

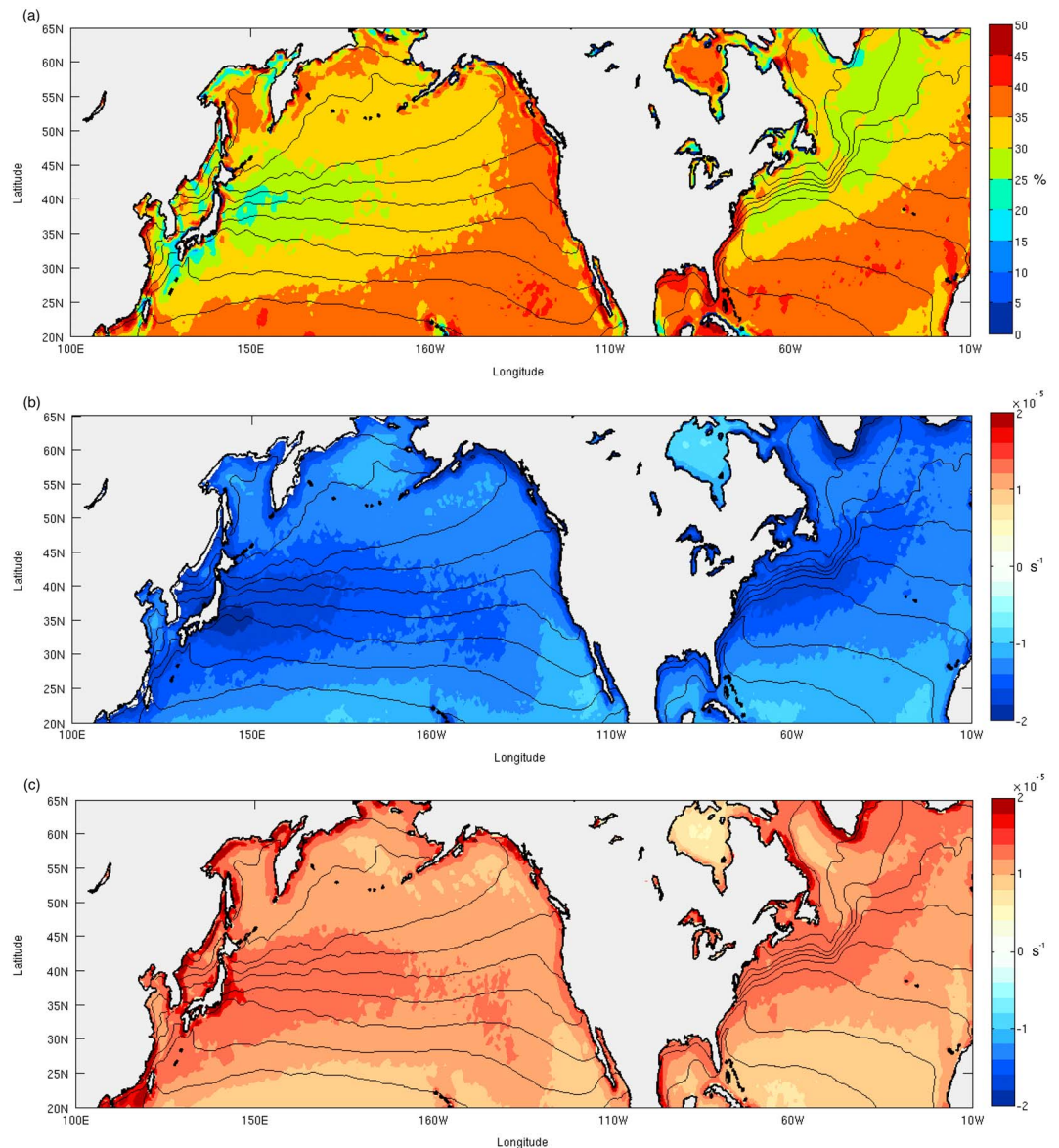


Figure 3. (a) The percentage of atmospheric non-frontal days for the period December–February 1979–2010 where near-surface wind convergence (as opposed to near-surface wind divergence) is identified at each grid point. (b) The time-mean near-surface wind convergence/divergence field for those atmospheric non-frontal days where near-surface wind convergence only is identified. (c) The time-mean near-surface wind convergence/divergence field for those atmospheric non-frontal days where near-surface wind divergence only is identified.

tropospheric potential vorticity anomalies such as these are observed within synoptic storm systems in the KE and GS regions—see Figure 3.17 in Parfitt (2014).

2. The diabatic contribution taking place at atmospheric fronts (Emanuel, 1985) which offers much less cancellation (cf. Figure 1; Green et al., 1966). This is illustrated schematically in supporting information Figure S2b. The removal of this atmospheric frontal contribution leaves on average NSWD, which is a view reminiscent of that put forward in the tropics regarding the impact of convection on large-scale circulations (Emanuel et al., 1994; Yanai et al., 1973).

As mentioned previously, atmospheric fronts exist over the KE and GS up to ~25% of the time in wintertime, meaning that the atmospheric non-frontal regime exists over ~75% of the time. If one defines q_n as the atmospheric frontal frequency, c_n as the average atmospheric frontal NSWC/NSWD (Figure 2a), and d_n as the

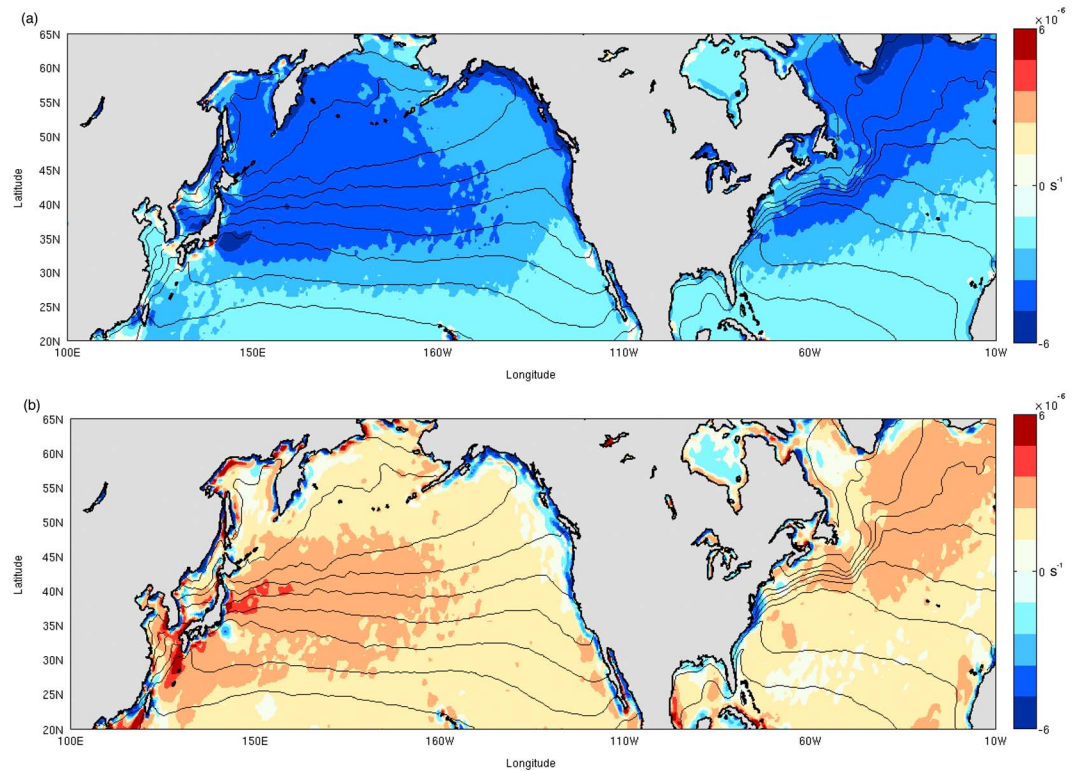


Figure 4. (a) The product of the atmospheric frontal frequency (as a fraction of the total period December–February 1979–2010) and the average near-surface wind convergence/divergence field when atmospheric fronts only are present. (b) The product of the atmospheric non-frontal frequency (i.e., the fraction of time that atmospheric fronts are not present) and the average near-surface wind convergence/divergence field when atmospheric fronts are not present. Panels (a) and (b) represent the weighted contribution of atmospheric frontal and non-frontal scenarios to the total time-mean near-surface wind convergence/divergence field.

average atmospheric non-frontal NSWC/NSWD (Figure 2c) at grid point n , then the mean NSWC/NSWD in Figures 1a and 1b is by definition calculated at each grid point n as $q_n c_n + (1 - q_n) d_n$. In other words, significant areas of average NSWC generally observed toward the warmer SSTs of the KE and GS in Figure 1 simply arise because at those points the contribution from $q_n c_n$ is greater than that from $(1 - q_n) d_n$, meaning that the average atmospheric frontal NSWC/NSWD in Figure 2a is enough to dominate over the average non-frontal NSWC/NSWD in Figure 2c. This can be clearly seen in Figure 4, which plots (a) $q_n c_n$ and (b) $(1 - q_n) d_n$. It was noted previously that the difference in atmospheric frontal NSWC magnitude c_n between the warm and cold sides of the GS is observed to be more prominent than between the warm and cold sides of the KE (Figure 2a). However, multiplying by q_n as in Figure 4a to obtain the total weighted atmospheric frontal contribution to the time-mean can be seen to recover the strong maxima in NSWC toward the warm side of the KE in the time-mean. This is consistent with Parfitt et al. (2016) and Parfitt, Czaja, and Kwon (2017), who showed in the GS region that one expects a stronger intensification of atmospheric fronts from a sharp SST gradient to manifest toward the warmer side of the SST front.

4. Discussion

For the past few decades, it has been known that the time-mean NSWC in the KE and GS regions exhibits a strong imprint of the oceanic fronts. Many potential mechanisms have been put forward to explain this phenomenon in the time-mean, in particular the pressure adjustment mechanism, whereby the Laplacians of SST and sea level pressure are shown to meander with the NSWC/NSWD. However, one issue with this interpretation based on steady Ekman layer dynamics is the presence of a transient baroclinic waveguide that exists at these latitudes along which a continuous series of synoptic systems propagates. In the last few years, studies have suggested that the time-mean NSWC/NSWD in the KE and GS regions on the

order of 10^{-6} s^{-1} (cf. Figure 1) are heavily skewed by these synoptic systems which are expected to have vastly different NSWC/NSWD patterns with values over an order of magnitude larger (O'Neill et al., 2017; Parfitt & Czaja, 2016). As a result, on a daily timescale it is difficult to understand from where the meandering oceanic imprint on the time-mean NSWC/NSWD pattern originates. This study has introduced a new framework to resolve this apparent disagreement, by illustrating the usefulness of partitioning the NSWC/NSWD field specifically into atmospheric frontal and non-frontal components of the baroclinic waveguide. Removal of atmospheric fronts, for which there is on average only NSWC on the order of 10^{-5} s^{-1} , leaves on average only NSWD on the order of 10^{-6} s^{-1} . Further decomposition of this average atmospheric non-frontal NSWD into the contributing NSWC-only and NSWD-only averages illustrates that this non-frontal NSWD is, in fact, a sum of non-frontal NSWCs and NSWDs an order of magnitude larger, suggesting this non-frontal motion can be attributed to the isentropic upglide and downglide found within a baroclinic waveguide.

This new framework prompts interesting new questions regarding the role of SST forcing by the KE and GS on the time-mean atmospheric state. For example, do the atmospheric frontal and non-frontal averages in Figures 2a and 2b indicate that any overall SST forcing of the time-mean NSWC/NSWD field is simply a result of an increase in atmospheric frontal convergence? While the interaction between the KE and GS SST fronts and atmospheric fronts is little explored, there is an existing theory that attributes an increase in atmospheric frontal activity across the KE and GS SST fronts to the surface sensible heat flux gradient across the strong SST gradients (TDS, Parfitt et al., 2016). Nevertheless, Figure 3a illustrates that over the KE and GS, atmospheric non-frontal NSWD occurs more frequently than non-frontal NSWC. In order for cancellation to an order of magnitude lower in the non-frontal time-mean (Figure 2c), the non-frontal NSWC over the KE and GS must necessarily be larger. Two mechanisms have already been suggested to explain part of the increase in non-frontal NSWC related to the KE and GS (*cold path*: Vannière et al., 2017, and *warm path*: Sheldon et al., 2017). Therefore, while the KE and GS may indeed act to increase non-frontal NSWC, Figure 2c suggests that their *overall* effect in non-frontal scenarios may simply be to increase NSWC such that in the *time-mean* it cancels more exactly with non-frontal NSWD, resulting in a weak signal.

Finally, distinct to the atmospheric frontal TDS mechanism above, which relies on sensible heat flux gradients, the components of the cold-path and warm-path mechanisms applicable to non-frontal situations rely heavily on absolute SST and latent heat flux anomalies. In the past few decades, modeling studies have championed the dominance of both sensible (e.g., Hotta & Nakamura, 2011) and latent (e.g., Booth et al., 2012) heating on the Northern Hemisphere storm-tracks, although a general consensus is still lacking. Perhaps a reason for this is that very few modeling studies have discussed sensible and latent heating responses in the context of atmospheric frontal and non-frontal situations independently, which have been shown here to imprint distinctively on the atmospheric NSWC/NSWD field. To the authors' knowledge, there is no study comparing the relative sensitivity of atmospheric fronts to SST gradient, absolute SST and SST orientation in one model configuration. Our results suggest a comprehensive study of that nature, which would accurately test the importance of the cross atmospheric frontal sensible heat flux gradient to atmospheric non-frontal latent heating, may be the key to quantifying the processes impacting the atmospheric response to the KE and GS. This work is currently being undertaken by the authors using regional modeling experiments as well as a suite of high-resolution general circulation models.

Acknowledgments

We gratefully acknowledge the support from the NSF Physical Oceanography program (OCE-1419235 and AGS-1355339). NCEP-CFSR is a publicly available data set and is accessible at <https://rda.ucar.edu/datasets/ds093.0/>. We would like to thank NCAR for allowing access to the NCEP-CFSR data set.

References

- Bishop, S. P., Small, R. J., Bryan, F. O., & Tomas, R. A. (2017). Scale dependence of midlatitude air–sea interaction. *Journal of Climate*, *30*(20), 8207–8221. <https://doi.org/10.1175/JCLI-D-17-0159.1>
- Booth, J. F., Thompson, L., Patoux, J., & Kelly, K. A. (2012). Sensitivity of midlatitude storm intensification to perturbations in the sea surface temperature near the Gulf Stream. *Monthly Weather Review*, *140*(4), 1241–1256. <https://doi.org/10.1175/MWR-D-11-00195.1>
- Catto, J. L., Jakob, C., Berry, G., & Nicholls, N. (2012). Relating global precipitation to atmospheric fronts. *Geophysical Research Letters*, *39*, L10805. <https://doi.org/10.1029/2012GL051736>
- Chang, E. K., Lee, S., & Swanson, K. L. (2002). Storm track dynamics. *Journal of Climate*, *15*(16), 2163–2183. [https://doi.org/10.1175/1520-0442\(2002\)015<02163:STD>2.0.CO;2](https://doi.org/10.1175/1520-0442(2002)015<02163:STD>2.0.CO;2)
- Chelton, D. B., Schlax, M. G., Freilich, M. H., & Milliff, R. F. (2004). Satellite measurements reveal persistent small-scale features in ocean winds. *Science*, *303*(5660), 978–983. <https://doi.org/10.1126/science.1091901>
- Emanuel, K. A. (1985). Frontal circulations in the presence of small moist symmetric stability. *Journal of the Atmospheric Sciences*, *42*(10), 1062–1071. [https://doi.org/10.1175/1520-0469\(1985\)042<1062:FCITPO>2.0.CO;2](https://doi.org/10.1175/1520-0469(1985)042<1062:FCITPO>2.0.CO;2)
- Emanuel, K. A., Neelin, J. D., & Bretherton, C. S. (1994). On large-scale circulations in convecting atmospheres. *Quarterly Journal of the Royal Meteorological Society*, *120*(519), 1111–1143. <https://doi.org/10.1002/qj.49712051902>

- Feliks, Y., Ghil, M., & Simonnet, E. (2004). Low-frequency variability in the midlatitude atmosphere induced by an oceanic thermal front. *Journal of the Atmospheric Sciences*, *61*(9), 961–981. [https://doi.org/10.1175/1520-0469\(2004\)061<0961:LVTMA>2.0.CO;2](https://doi.org/10.1175/1520-0469(2004)061<0961:LVTMA>2.0.CO;2)
- Feliks, Y., Ghil, M., & Simonnet, E. (2007). Low-frequency variability in the midlatitude baroclinic atmosphere induced by an oceanic thermal front. *Journal of the Atmospheric Sciences*, *64*(1), 97–116. <https://doi.org/10.1175/JAS3780.1>
- Green, J. S. A., Ludlam, F. H., & McIlveen, J. F. R. (1966). Isentropic relative-flow analysis and the parcel theory. *Quarterly Journal of the Royal Meteorological Society*, *92*(392), 210–219. <https://doi.org/10.1002/qj.49709239204>
- Hand, R., Keenlyside, N., Omrani, N. E., & Latif, M. (2014). Simulated response to inter-annual SST variations in the Gulf stream region. *Climate Dynamics*, *42*(3–4), 715–731. <https://doi.org/10.1007/s00382-013-1715-y>
- Hayes, S. P., McPhaden, M. J., & Wallace, J. M. (1989). The influence of sea-surface temperature on surface wind in the eastern equatorial Pacific: Weekly to monthly variability. *Journal of Climate*, *2*(12), 1500–1506. [https://doi.org/10.1175/1520-0442\(1989\)002<1500:TIOSS>2.0.CO;2](https://doi.org/10.1175/1520-0442(1989)002<1500:TIOSS>2.0.CO;2)
- Hewson, T. D. (1998). Objective fronts. *Meteorological Applications*, *5*(1), 37–65. <https://doi.org/10.1017/S1350482798000553>
- Hirata, H., Kawamura, R., Kato, M., & Shinoda, T. (2015). Influential role of moisture supply from the Kuroshio/Kuroshio Extension in the rapid development of an extratropical cyclone. *Monthly Weather Review*, *143*(10), 4126–4144. <https://doi.org/10.1175/MWR-D-15-0016.1>
- Hirata, H., Kawamura, R., Kato, M., & Shinoda, T. (2018). A positive feedback process related to the rapid development of an extratropical cyclone over the Kuroshio/Kuroshio Extension. *Monthly Weather Review*, *146*(2), 417–433. <https://doi.org/10.1175/MWR-D-17-0063.1>
- Hoskins, B., Pedder, M., & Jones, D. W. (2003). The omega equation and potential vorticity. *Quarterly Journal of the Royal Meteorological Society*, *129*(595), 3277–3303. <https://doi.org/10.1256/qj.02.135>
- Hotta, D., & Nakamura, H. (2011). On the significance of the sensible heat supply from the ocean in the maintenance of the mean baroclinicity along storm tracks. *Journal of Climate*, *24*(13), 3377–3401. <https://doi.org/10.1175/2010JCLI3910.1>
- Joyce, T. M., Kwon, Y. O., & Yu, L. (2009). On the relationship between synoptic wintertime atmospheric variability and path shifts in the Gulf Stream and the Kuroshio Extension. *Journal of Climate*, *22*(12), 3177–3192. <https://doi.org/10.1175/2008JCLI2690.1>
- Kilpatrick, T., Schneider, N., & Qiu, B. (2014). Boundary layer convergence induced by strong winds across a midlatitude SST front. *Journal of Climate*, *27*(4), 1698–1718. <https://doi.org/10.1175/JCLI-D-13-00101.1>
- Kobashi, F., Xie, S. P., Iwasaka, N., & Sakamoto, T. T. (2008). Deep atmospheric response to the North Pacific oceanic subtropical front in spring. *Journal of Climate*, *21*(22), 5960–5975. <https://doi.org/10.1175/2008JCLI2311.1>
- Kuwano-Yoshida, A., & Minobe, S. (2017). Storm-track response to SST fronts in the northwestern Pacific region in an AGCM. *Journal of Climate*, *30*(3), 1081–1102. <https://doi.org/10.1175/JCLI-D-16-0331.1>
- Lindzen, R. S., & Nigam, S. (1987). On the role of sea surface temperature gradients in forcing low-level winds and convergence in the tropics. *Journal of the Atmospheric Sciences*, *44*(17), 2418–2436. [https://doi.org/10.1175/1520-0469\(1987\)044<2418:OTROSS>2.0.CO;2](https://doi.org/10.1175/1520-0469(1987)044<2418:OTROSS>2.0.CO;2)
- Liu, J. W., Zhang, S. P., & Xie, S. P. (2013). Two types of surface wind response to the East China Sea Kuroshio front. *Journal of Climate*, *26*(21), 8616–8627. <https://doi.org/10.1175/JCLI-D-12-00092.1>
- Ma, X., Jing, Z., Chang, P., Liu, X., Montuoro, R., Small, R. J., et al. (2016). Western boundary currents regulated by interaction between ocean eddies and the atmosphere. *Nature*, *535*(7613), 533–537. <https://doi.org/10.1038/nature18640>
- Messori, G., Geen, R., & Czaja, A. (2017). On the spatial and temporal variability of atmospheric heat transport in a hierarchy of models. *Journal of the Atmospheric Sciences*, *74*(7), 2163–2189. <https://doi.org/10.1175/JAS-D-16-0360.1>
- Minobe, S., Kuwano-Yoshida, A., Komori, N., Xie, S. P., & Small, R. J. (2008). Influence of the Gulf stream on the troposphere. *Nature*, *452*(7184), 206–209. <https://doi.org/10.1038/nature06690>
- Minobe, S., Miyashita, M., Kuwano-Yoshida, A., Tokinaga, H., & Xie, S. P. (2010). Atmospheric response to the Gulf Stream: Seasonal variations. *Journal of Climate*, *23*(13), 3699–3719. <https://doi.org/10.1175/2010JCLI3359.1>
- Nakamura, H., Nishina, A., & Minobe, S. (2012). Response of storm tracks to bimodal Kuroshio path states south of Japan. *Journal of Climate*, *25*(21), 7772–7779. <https://doi.org/10.1175/JCLI-D-12-00326.1>
- Nkwinkwa Njoudo, A. S., Koseki, S., Keenlyside, N., & Rouault, M. (2018). Atmospheric signature of the Agulhas current. *Geophysical Research Letters*, *45*, 5185–5193. <https://doi.org/10.1029/2018GL077042>
- Nonaka, M., & Xie, S. P. (2003). Covariations of sea surface temperature and wind over the Kuroshio and its extension: Evidence for ocean-to-atmosphere feedback. *Journal of Climate*, *16*(9), 1404–1413. [https://doi.org/10.1175/1520-0442\(2003\)16<1404:COSSA>2.0.CO;2](https://doi.org/10.1175/1520-0442(2003)16<1404:COSSA>2.0.CO;2)
- O'Neill, L. W., Haack, T., Chelton, D. B., & Skillingstad, E. (2017). The Gulf Stream Convergence Zone in the time-mean winds. *Journal of the Atmospheric Sciences*, *74*(7), 2383–2412. <https://doi.org/10.1175/JAS-D-16-0213.1>
- O'Neill, L. W., Haack, T., Chelton, D. B., & Skillingstad, E. (2018). Reply to “Comments on ‘The Gulf Stream Convergence Zone in the time-mean winds’”. *Journal of the Atmospheric Sciences*, *75*(6), 2151–2153. <https://doi.org/10.1175/JAS-D-18-0044.1>
- Parfitt, R. (2014). Extreme air-sea interactions over the Gulf Stream, (PhD thesis, pp. 189). London: Imperial College.
- Parfitt, R., & Czaja, A. (2016). On the contribution of synoptic transients to the mean atmospheric state in the Gulf Stream region. *Quarterly Journal of the Royal Meteorological Society*, *142*(696), 1554–1561. <https://doi.org/10.1002/qj.2689>
- Parfitt, R., Czaja, A., & Kwon, Y. O. (2017). The impact of SST resolution change in the ERA-Interim reanalysis on wintertime gulf stream frontal air-sea interaction. *Geophysical Research Letters*, *44*, 3246–3254. <https://doi.org/10.1002/2017GL073028>
- Parfitt, R., Czaja, A., Minobe, S., & Kuwano-Yoshida, A. (2016). The atmospheric frontal response to SST perturbations in the Gulf Stream region. *Geophysical Research Letters*, *43*, 2299–2306. <https://doi.org/10.1002/2016GL067723>
- Parfitt, R., Czaja, A., & Seo, H. (2017). A simple diagnostic for the detection of atmospheric fronts. *Geophysical Research Letters*, *44*, 4351–4358. <https://doi.org/10.1002/2017GL073662>
- Piazza, M., Terray, L., Boé, J., Maisonnave, E., & Sanchez-Gomez, E. (2016). Influence of small-scale North Atlantic Sea surface temperature patterns on the marine boundary layer and free troposphere: A study using the atmospheric ARPEGE model. *Climate Dynamics*, *46*(5–6), 1699–1717. <https://doi.org/10.1007/s00382-015-2669-z>
- Plougonven, R., Foussard, A., & Lapeyre, G. (2018). Comments on “The Gulf Stream Convergence Zone in the time-mean winds”. *Journal of the Atmospheric Sciences*, *75*(6), 2139–2149. <https://doi.org/10.1175/JAS-D-17-0369.1>
- Saha, S., Moorthi, S., Pan, H. L., Wu, X., Wang, J., Nadiga, S., et al. (2010). The NCEP Climate Forecast System Reanalysis. *Bulletin of the American Meteorological Society*, *91*(8), 1015–1058. <https://doi.org/10.1175/2010BAMS3001.1>
- Sasaki, Y. N., Minobe, S., Asai, T., & Inatsu, M. (2012). Influence of the Kuroshio in the East China Sea on the early summer (baiu) rain. *Journal of Climate*, *25*(19), 6627–6645. <https://doi.org/10.1175/JCLI-D-11-00727.1>
- Sasaki, Y. N., & Yamada, Y. (2017). Atmospheric response to interannual variability of sea surface temperature front in the East China Sea in early summer. *Climate Dynamics*, 1–14.
- Schneider, N., & Qiu, B. (2015). The atmospheric response to weak sea surface temperature fronts. *Journal of the Atmospheric Sciences*, *72*(9), 3356–3377. <https://doi.org/10.1175/JAS-D-14-0212.1>

- Seo, H., Kwon, Y.-O., Joyce, T. M., & Ummerhofer, C. C. (2017). On the predominant nonlinear response of the extratropical atmosphere to meridional shift of the Gulf Stream. *Journal of Climate*, *30*(23), 9679–9702. <https://doi.org/10.1175/JCLI-D-16-0707.1>
- Sheldon, L., Czaja, A., Vannière, B., Morcrette, C., Sohet, B., Casado, M., et al. (2017). A “warm path” for Gulf Stream–troposphere interactions. *Tellus A: Dynamic Meteorology and Oceanography*, *69*(1), 1299397. <https://doi.org/10.1080/16000870.2017.1299397>
- Shimada, T., & Minobe, S. (2011). Global analysis of the pressure adjustment mechanism over sea surface temperature fronts using AIRS/Aqua data. *Geophysical Research Letters*, *38*, L06704. <https://doi.org/10.1029/2010GL046625>
- Small, R. J., Msadek, R., Kwon, Y. O., Booth, J. F., & Zarzycki, C. (2018). Atmosphere surface storm track response to resolved ocean mesoscale in two sets of global climate model experiments. *Climate Dynamics*, 1–23.
- Small, R. J., Tomas, R. A., & Bryan, F. O. (2014). Storm track response to ocean fronts in a global high-resolution climate model. *Climate Dynamics*, *43*(3–4), 805–828. <https://doi.org/10.1007/s00382-013-1980-9>
- Small, R. J., Xie, S. P., O'Neill, L., Seo, H., Song, Q., Cornillon, P., et al. (2008). Air–sea interaction over ocean fronts and eddies. *Dynamics of Atmospheres and Oceans*, *45*(3–4), 274–319. <https://doi.org/10.1016/j.dynatmoce.2008.01.001>
- Solman, S., & Orlanski, I. (2010). Subpolar high anomaly preconditioning precipitation over South America. *Journal of the Atmospheric Sciences*, *67*(5), 1526–1542. <https://doi.org/10.1175/2009JAS3309.1>
- Taguchi, B., Nakamura, H., Nonaka, M., & Xie, S. P. (2009). Influences of the Kuroshio/Oyashio Extensions on air–sea heat exchanges and storm-track activity as revealed in regional atmospheric model simulations for the 2003/04 cold season. *Journal of Climate*, *22*(24), 6536–6560. <https://doi.org/10.1175/2009JCLI2910.1>
- Tokinaga, H., Tanimoto, Y., Xie, S. P., Sampe, T., Tomita, H., & Ichikawa, H. (2009). Ocean frontal effects on the vertical development of clouds over the western North Pacific: In situ and satellite observations. *Journal of Climate*, *22*(16), 4241–4260. <https://doi.org/10.1175/2009JCLI2763.1>
- Vannière, B., Czaja, A., Dacre, H., & Woollings, T. (2017). A “cold path” for the Gulf Stream–troposphere connection. *Journal of Climate*, *30*(4), 1363–1379. <https://doi.org/10.1175/JCLI-D-15-0749.1>
- Wai, M. M. K., & Stage, S. A. (1989). Dynamical analyses of marine atmospheric boundary layer structure near the Gulf stream oceanic front. *Quarterly Journal of the Royal Meteorological Society*, *115*(485), 29–44. <https://doi.org/10.1002/qj.49711548503>
- Wallace, J. M., Lim, G. H., & Blackmon, M. L. (1988). Relationship between cyclone tracks, anticyclone tracks and baroclinic waveguides. *Journal of the Atmospheric Sciences*, *45*(3), 439–462. [https://doi.org/10.1175/1520-0469\(1988\)045<0439:RBCTAT>2.0.CO;2](https://doi.org/10.1175/1520-0469(1988)045<0439:RBCTAT>2.0.CO;2)
- Wallace, J. M., Mitchell, T. P., & Deser, C. (1989). The influence of sea-surface temperature on surface wind in the eastern equatorial Pacific: Seasonal and interannual variability. *Journal of Climate*, *2*(12), 1492–1499. [https://doi.org/10.1175/1520-0442\(1989\)002<1492:TIOSST>2.0.CO;2](https://doi.org/10.1175/1520-0442(1989)002<1492:TIOSST>2.0.CO;2)
- Xie, S. P. (2004). Satellite observations of cool ocean–atmosphere interaction. *Bulletin of the American Meteorological Society*, *85*(2), 195–208. <https://doi.org/10.1175/BAMS-85-2-195>
- Yanai, M., Esbensen, S., & Chu, J. H. (1973). Determination of bulk properties of tropical cloud clusters from large-scale heat and moisture budgets. *Journal of the Atmospheric Sciences*, *30*(4), 611–627. [https://doi.org/10.1175/1520-0469\(1973\)030<0611:DOBPO>2.0.CO;2](https://doi.org/10.1175/1520-0469(1973)030<0611:DOBPO>2.0.CO;2)



Geophysical Research Letters

Supporting Information for

A New Framework for Near-Surface Wind Convergence over the Kuroshio Extension and Gulf Stream in Wintertime: The Role of Atmospheric Fronts

Rhys Parfitt and Hyodae Seo

Woods Hole Oceanographic Institution

Contents of this file

Figures S1 to S2

Introduction

This file contains Supplementary Figures 1-2, along with the associated captions.

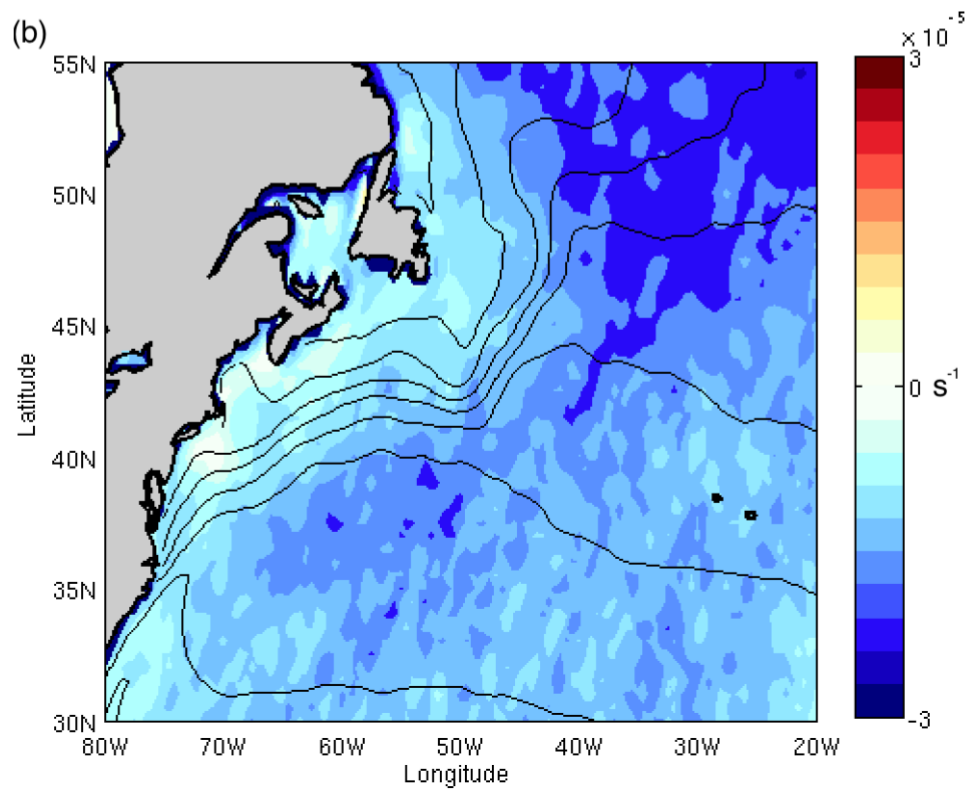
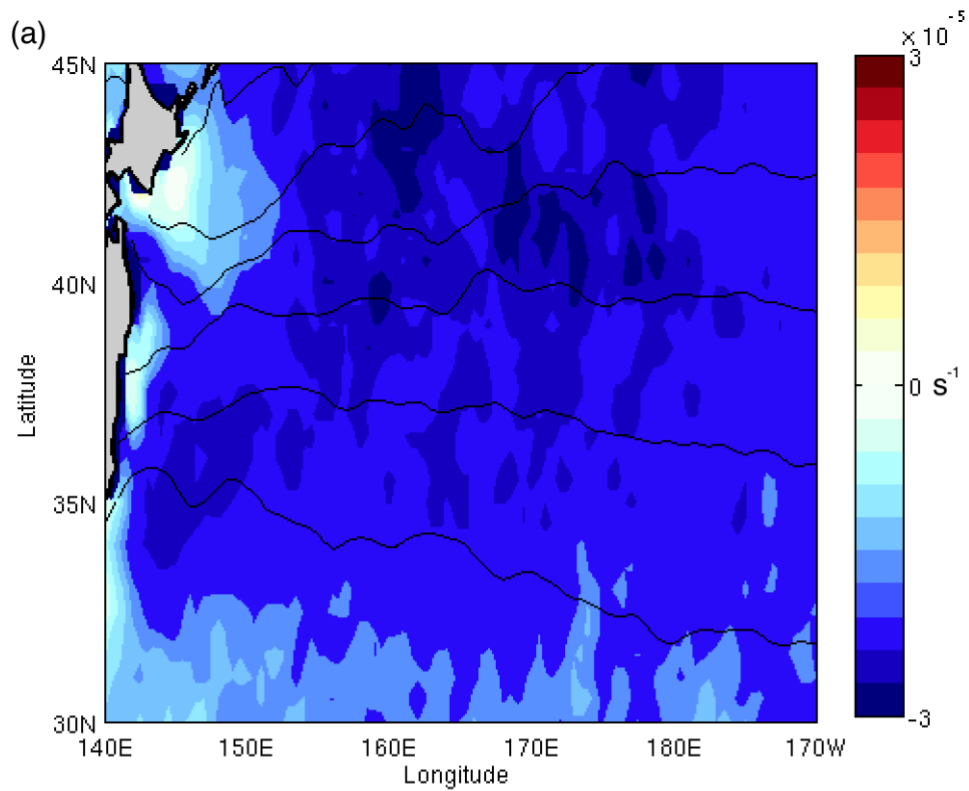


Figure S1: The time-mean near-surface wind convergence/divergence field over the (a) Kuroshio Extension and (b) Gulf Stream when atmospheric fronts only are present. These are regional maps of the field shown in Figure 2(a), with enhanced scale resolution.

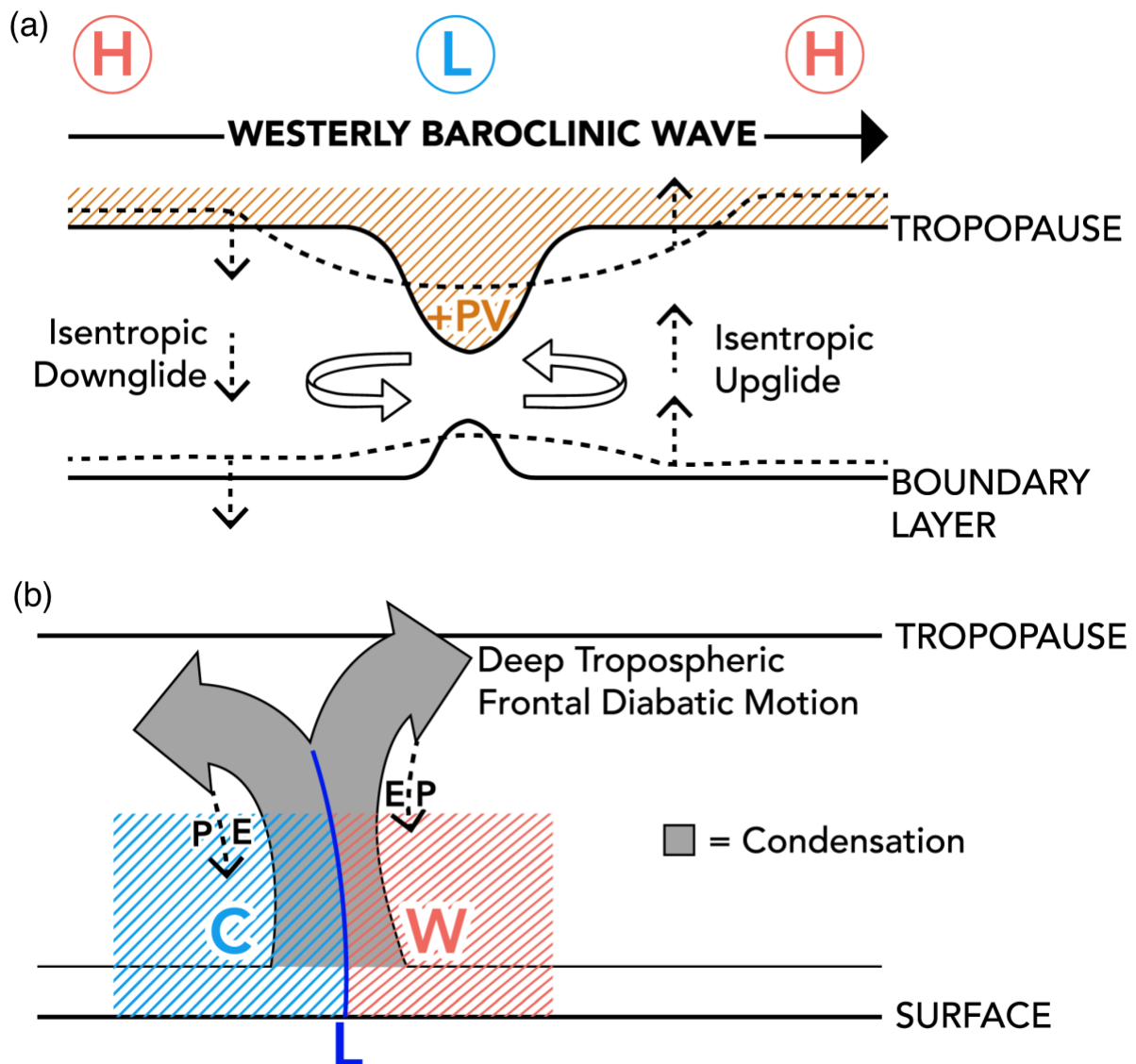


Figure S2: (a) Schematic illustrating the effect of a positive potential vorticity δ -function superimposed on a westerly baroclinic flow. The dashed lines represent isentropes with the vertical dashed arrows illustrating the vertical motion associated with isentropic upglide and downglide. The horizontal curved arrows depict the horizontal circulation. This type of sharp potential vorticity anomaly is commonly found in the centre of extra-tropical cyclones, as a dip in the tropopause brings high stratospheric PV downwards. Figure adapted from Figure 1 in Hoskins et al. (2003) and Figure 3.17 in Parfitt (2014). (b) Schematic illustrating deep tropospheric motion at an atmospheric cold front (cold and warm air in blue and red respectively), projected on a vertical section. The low pressure centre is denoted by L. Condensation occurs where there is shading, precipitation P falls from the induced cloud-system and there is some evaporation E outside of it. Figure adapted from Figure 1 in Green et al. (1966).